CFD MODELLING OF PLUME INTERACTION IN NATURAL VENTILATION

Faisal Durrani[1], Malcolm J Cook[1], James J McGuirk[2] and Nigel B Kaye[3]
[1]Department of Civil and Building Engineering, Loughborough University, LE11 3TU, UK
[2]Department of Aeronautical and Automotive Engineering, Loughborough University, LE11 3TU, UK
[3]Civil Engineering, Clemson University, Clemson, SC 29634, USA

ABSTRACT

This paper investigates the accuracy of CFD simulation in predicting the nature of multiple plume interactions in a naturally ventilated indoor environment. RANS-based turbulence models; k-ε and RNG k-ε were used to predict the twin plume interaction experiment reported by Kaye and Linden (2004). It was observed that the k-ε turbulence model showed a large discrepancy with measurements while the results obtained from the RNG k-ε model were in better accord with the experimental results. A grid sensitivity analysis of the computational solution also formed part of this study.

INTRODUCTION

Natural ventilation is being increasingly incorporated into many new low energy building designs. Anderson (1995), Awbi & Gan (1992), Bansal et al. (1993), Barozzi et al. (1992), Bouchair (1993), Van der Mass & Roulet (1991) and Tan (2000) reported that buoyancy-driven natural ventilation is one of the most favoured strategies for natural ventilation design. Buoyancy-driven natural ventilation harnesses the buoyancy forces associated with the temperature differences between the interior and exterior environments to drive air flow through a building.

This paper reports on a study that investigated the use of RANS-based turbulence models for modelling buoyancy-driven flows in naturally ventilated buildings. Ventilated enclosures with multiple heat sources contain turbulent plumes that rise above the heat sources and interact with each other. Linden (1999) reports that this interaction affects the behaviour of the resulting ventilation flow. The behaviour of plumes in the built environment have been analyzed by Kaye and Linden (2004). The experimental results obtained from their paper are used here to help select a suitable RANS-based turbulence model for predicting the behaviour of such plumes.

ANALYTICAL AND EXPERIMENTAL WORK

Buoyancy-driven natural ventilation was studied by Linden et al. (1990). The experimental work considered displacement ventilation driven by a continuous point source of buoyancy on the floor. It was observed that steady stratification was produced consisting of two homogeneous layers of fluid separated by a horizontal interface at a height *h* above the floor. The lower layer of fluid was at ambient temperature while the upper layer was at a temperature equal to the plume temperature at height *h* (see Fig. 1). The steady interface is formed where the volume and buoyancy fluxes through the upper openings equal that supplied to the upper layer by the plume.

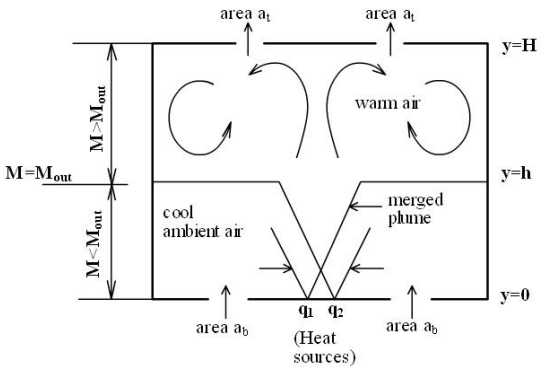

Figure 1 Schematic representation of steady natural ventilation flow in an enclosure with notation.

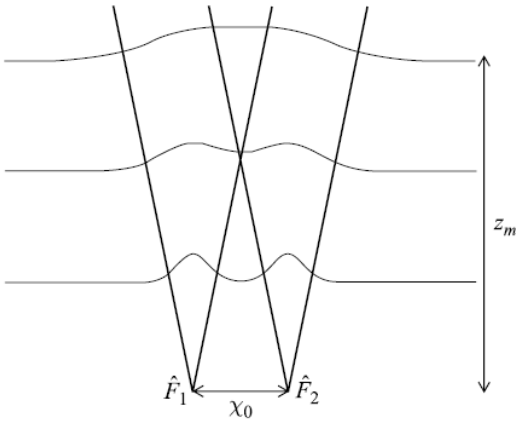

Figure 2 Schematic of two plumes showing merging height Z_m and the plume separation X_o (source: Kaye, 2004)

Pera & Gebhart (1975) have shown that the problem of merging of two co-flowing fully turbulent plumes with sources at the same level is primarily dependent

on the buoyancy fluxes $\hat{F}_1$and $\hat{F}_2$ (with $\hat{F}_1 \geq \hat{F}_2$ by convention) and the source separation X_0.

Plume merge height was found to be a function only of these parameters. If z_m is the height at which the plumes merge then (Kaye, 2004) (see Fig. 2):

$$\frac{z_m}{X_0} = func\left(\frac{\hat{F}_1}{\hat{F}_2}\right) \qquad (1)$$

The scenario considered for this study is that of a single space enclosure (Figure 1), with high and low-level openings for air flow and with two sources of buoyancy with a buoyancy flux ratio $\psi = \frac{\hat{F}_2}{\hat{F}_1} = 0.45$.

These values are chosen in order to compare the predicted flow rates from CFD simulation with the experimental data reported by Kaye and Linden (2004) for the same buoyancy flux ratio.

In order to estimate the plume flow rates it was desired that the horizontal interface be formed somewhere above the plume merge height z_m but below the ceiling of the enclosure i.e. $z_m < h < H$. This was done using equations (2) and (3) to set the "effective" opening area *A**, as defined by Hunt and Linden (2001) , to give the required normalised interface height $\xi = h/H$, as defined by Linden el al. (1990).

$$A^* = \frac{C_D\, a_t a_b}{\left(\frac{1}{2}\left(\left(C_D{}^2/C_e\right)a_t + a_b{}^2\right)\right)^{\frac{1}{2}}} \qquad (2)$$

The quantities C_e and C_D are the coefficients of expansion and discharge respectively.

$$\frac{A^*}{H^2} = C^{3/2}\left[\frac{\xi^2}{1-\xi}\right] \qquad (3)$$

where,

$$C = \frac{6\alpha\left[\frac{9\alpha}{10}\right]^{1/3}\pi^{2/3}}{5} \qquad (4)$$

is dependent upon the entrainment coefficient α for the plume. Here 0.1 has been taken for the value of α in accordance with the work by Linden et al. (1990).

METHODOLOGY

Description of the Computational Domain

Many pre-test runs were performed to ensure that the horizontal interface and plume merging height did not come into contact. The computational domain was a rectangular enclosure with a floor area 25m^2 and height 5m. A view of the domain is shown in Figure 3.

Boundary conditions

The solution domain consists of symmetric placement of air inlets and outlets situated on the floor and roof respectively. Two heat sources of strengths q_1=50W and q_2=111.11W were also placed on the floor.

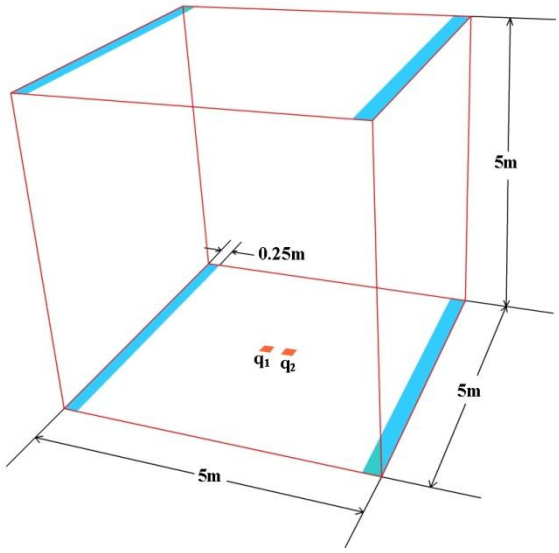

Figure 3 The Computational Domain (ventilation openings are shown in blue)

The enclosure was ventilated by a pair of two symmetrically positioned openings at the bottom and at the top. Each bottom opening had a total free area of a_b = 1.25 m^2 through which ambient air could enter the domain. Each top opening had a total area a_t = 1.25 m^2 through which the warmer air would exit the domain. The boundary condition assigned to both the top and bottom openings permits the fluid to cross the boundary in either direction according to the pressure loss defined by PHOENICS (2009):

$$\Delta P_{loss} = 0.5 \times K_L \times \rho \times vel^2 \qquad (5)$$

where K_L is the loss coefficient and is related to the discharge coefficient C_d as: $K_L=[1/(C_D)^2]$. A loss coefficient of 2.69 (C_D = 0.61) was used in this work.

The two heat sources had an area A = 0.0081 m^2 each and were positioned symmetrically on the floor separated by a horizontal distance *Xo* =0.4m.

To ensure that the plume would evolve in a stagnant flow and the stratified flow would develop quickly the following two initial conditions were imposed.

a) The three velocity components were set to zero

b) The temperature was set equal to the ambient temperature

The software package used for the CFD simulations was PHOENICS (2009) which uses the finite volume solution method on a staggered grid with a structured cartesian coordinate system. The Boussinesq approximation is used to represent buoyancy effects and the simulation was undertaken in steady state.

The simulation was considered to be converged when the global convergence criterion of 0.0001% was achieved.

Grid Refinement

A preliminary study was carried out where the grid was systematically refined to examine numerical accuracy aspects. The required grid density for grid independence depends mainly on the spatial *discretisation* technique selected for the non-linear convection terms. For the current work, convection terms were discretized using the HYBRID-differencing scheme (HDS) that is used in PHOENICS by default. HDS switches between the Upwind-differencing scheme (UDS) and Central-differencing scheme (CDS), according to the relative size of the convective and diffusion fluxes across cell surfaces, characterised by a local cell Peclet number Pe. CDS (second order accurate) is used for Pe < 2 while UDS (first order accurate) is used for Pe > 2. The cell Peclet number is the ratio of the convective to diffusive fluxes across a cell surface,

$$Pe = \frac{VxL}{\alpha}$$

where L is the local cell dimension, V is the local cell velocity, and α is the relevant diffusion coefficient (total (i.e. molecular + turbulent) viscosity for momentum and thermal diffusivity for temperature).
A coarse grid, to procure a solution quickly and establish confidence in the boundary conditions and solution domain size, was first selected. This was then refined to improve resolution in high gradient regions. The baseline grid size is referred to here as mesh A. In PHOENICS the baseline grid lines are distributed by the auto-mesher according to the following set of rules (PHOENICS User Documentation (2009)):

1. The maximum cell size is not allowed to exceed 5% of the domain size.
2. The ratio between the sizes of cells across region boundaries is not allowed to exceed a set limit (1.5). (A region is a user-defined zone in space containing a flow-significant 'object' – e.g. the regions of heat source on the floor or the slot openings in the floor/ceiling).
3. If the ratio is exceeded, the number of cells in a region is increased, and the spacing is set according to a geometrical progression using a set expansion ratio (1.2), until either the ratio criterion is satisfied at both ends of the region, or the cells at both ends are below a set minimum fraction (0.5%) of the domain size.

The baseline grid size was first doubled to produce a fine mesh density (mesh B). Refinement of the grid was then carried out specifically in areas where large gradients of solution variable (e.g. velocity or temperature) were identified in the mesh A solution. Failure to provide sufficient mesh density in these areas will result in the buoyant plume or the boundary layer flow being insufficiently resolved resulting in numerical smearing. Local grid refinement was carried out in particular on the edges of the rising plumes.

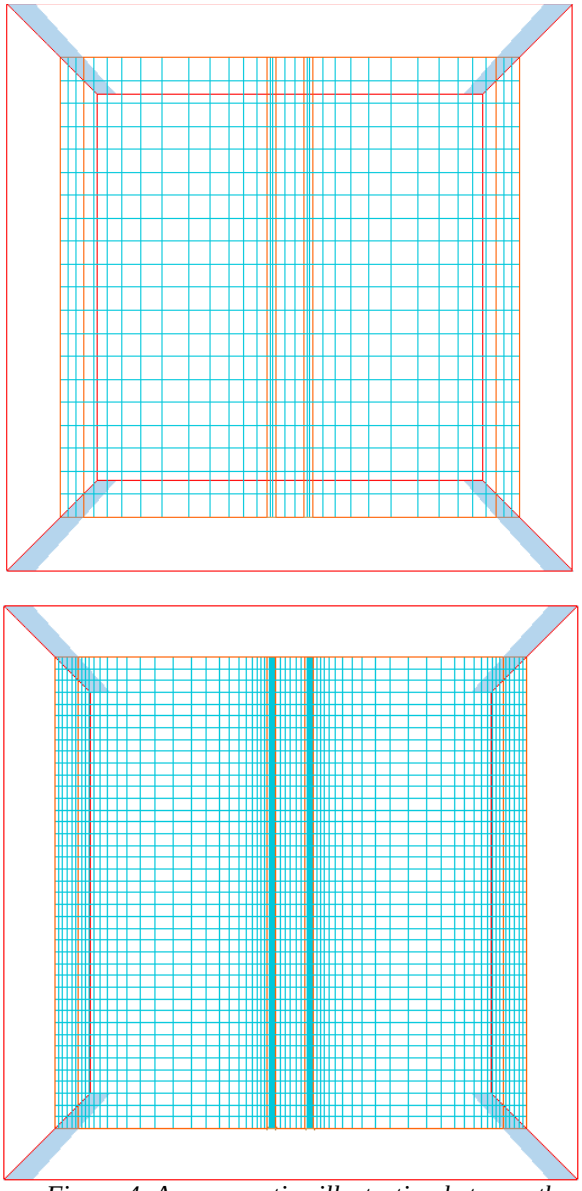

Figure 4: A comparative illustration between the coarse (top) and fine (bottom) mesh used

Figure 4 shows a sample of the mesh distribution in a horizontal plane, comparing meshes A and B. The parameter used to judge solution sensitivity to mesh refinement is the total volume flow rate Q in the rising plumes at a height z = 2.5m above the floor. Q was estimated as described above. The results are shown in Table 1 and Figure 5. Note that there is little variation in the estimated Q between the baseline grid and the two refined grids, implying that the baseline grid resolves the flow adequately.

Plume Flow rate estimation

Based on work by others (Murakami et al. (1996), Chen (1995), Murakami (1998) and Cook & Lomas (1997)) it was decided to study the performance of

the k-ε (Launder and Spalding, 1974) and RNG k- ε (Yakhot et al., 1992) models.

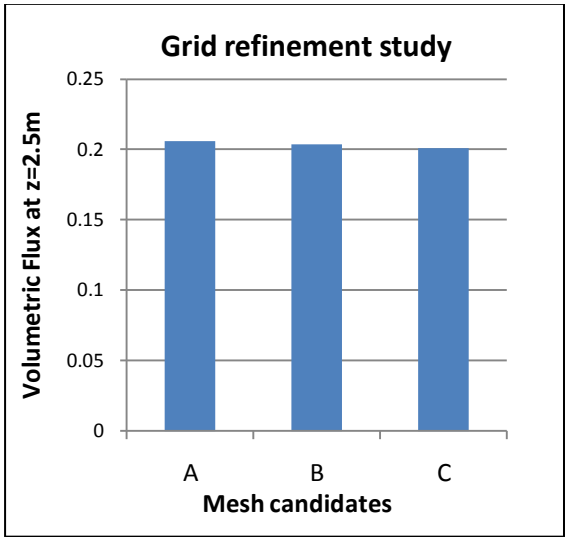

Figure 5: Grid Refinement study to achieve grid-independent solution

Mesh	Configuration	Q	total no. of cells	Grid size (x,y,z)
A	original	0.205	19980	(37,27,20)
B	2x overall	0.200	150960	(74,51,40)
C	2x source	0.203	25800	(43,30,20)

Table 1: Grid Mesh Settings and resulting Volumetric flows

Kaye and Linden (2004) focused on the far-field behaviour of the merged plumes by making a series of flow measurements in the merged plume, using the technique described by Baines (1983). The results were plotted in the form of non-dimensional height (*z/Xo*) versus the non-dimensional flow rate:

$$\frac{Q^{3/5}{F_1}^{-1/5}}{X_0}$$

The results were consistent with Baines (1983); the only difference is that all distances are scaled on the initial plume separation. Another difference is that rather than the sum of the two buoyancy fluxes the results are scaled in terms of F_1, the buoyancy flux in plume 1. The performance of the turbulence models was assessed based on their ability to accurately predict this relationship.

In order to calculate the local volume flux Q in the plume, velocity profiles obtained from our CFD simulations were plotted at different heights resulting in velocity profile curves as shown in figure 6. The volume flux Q can be calculated by integrating the area under the curve but in our study the profiles were assumed to be "top-hat" profiles which can be used to represent their Gaussian counterparts. This was done as it was in accordance with the approach adopted by Linden et al. (1990).

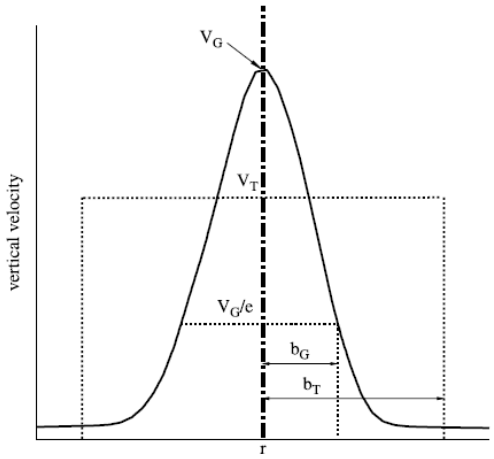

Figure 4 Velocity profile of a plume representing the Gaussian and "top-hat" profiles (source: Cook, 1998)

Here, b_G is the radial distance from the plume axis to the point at which the velocity has fallen to 1/e of the its axial value. The following two variables are also calculated using the numerical relationships between the top-hat quantities and their Gaussian counterparts, reported by Cook (1998):

$$b_T = \sqrt{2} b_G \quad (6)$$

$$v_T = \frac{v_G}{2} \quad (7)$$

Thus the volume flux can be calculated using the following equation:

$$Q = \pi \times {b_T}^2 \times v_T \quad (8)$$

Also,

$$\hat{F}_1 = \frac{2g\beta W_1}{\pi \rho C_p} \quad (9)$$

RESULTS

Qualitative Predictions

The flow pattern within the enclosure predicted by the CFD simulations is shown in Figure 7. The velocity vector plot shows the direction of the expanding and rising plume above the heat sources which spreads laterally on reaching the ceiling. Warm, buoyant air flows out through the upper openings and cool, ambient air is drawn in through the low-level openings. A contour plot of the velocity (figure 8) further supports this flow pattern.

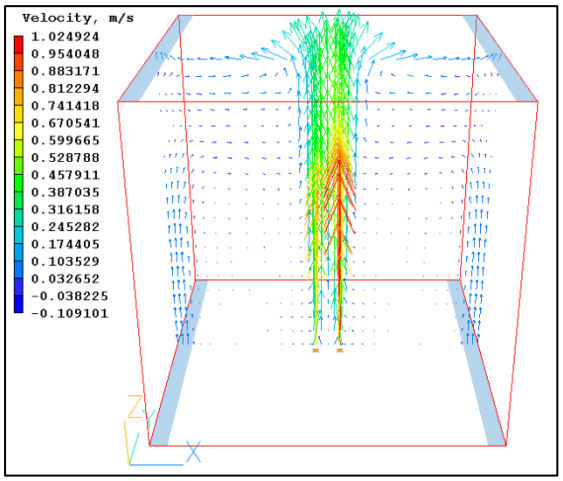

Figure 5 Velocity vector plot representing the flow directions inside the enclosure.

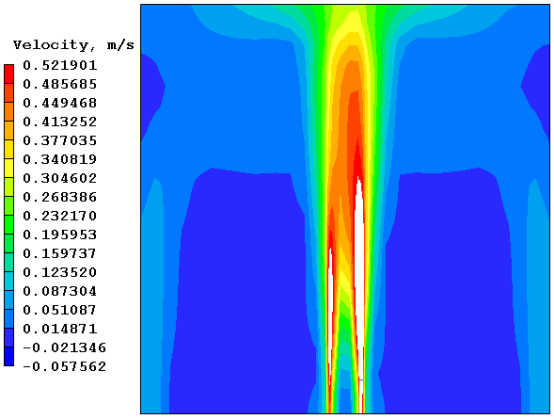

Figure 6 Velocity contours on a plane perpendicular to the heat sources, showing the coalescence of the two plumes.

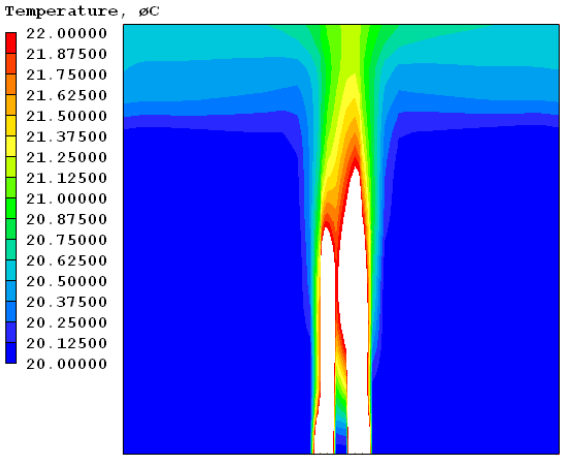

Figure 7 Temperature stratification inside the enclosure showing the two homogeneous fluid layers separated by the horizontal interface.

From the thermal stratification plot (figure 9), the formation of the two homogeneous layers of fluid separated by a horizontal interface is visible. It can also be observed that the upper layer is of the same temperature (approx. 20.4°C) while the lower temperature is approx. 20°C which is the ambient temperature. These results confirm the predictions of Linden et al. (1990).

Comparisons with experiments

The plot of the measured flow rates from experimental data and RANS-based models are shown in Figures 10 and 11. The black dotted lines represent the experimental data (with the change in gradient indicating the merge height) while the blue lines represent CFD predictions for particular turbulence models.

The first thing to observe from the CFD predictions is that they confirm the behaviour of a merged plume. The blue lines confirm the direct proportionality of the flow rates with the distance away from the buoyancy source.

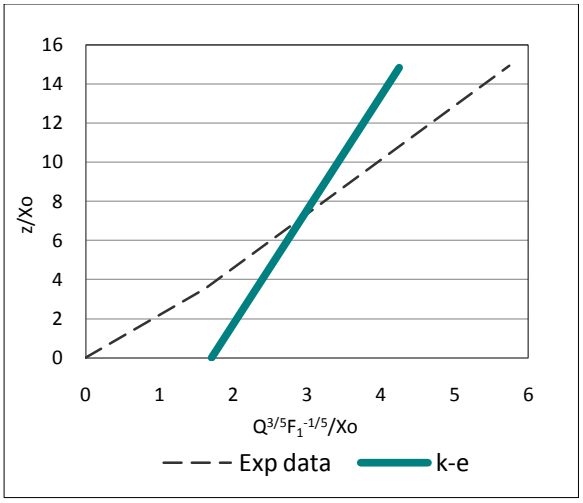

Figure 8 Prediction of the flow rates using the k- ε turbulence model compared to the flow rate measurements for two merging plumes with buoyancy flux ratio ψ=0.45.

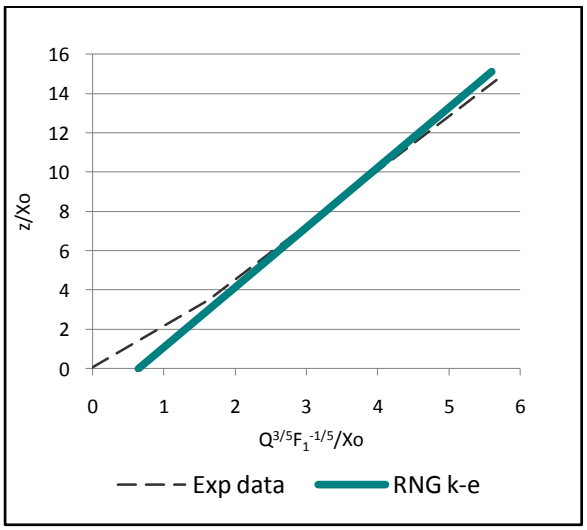

Figure 11 Prediction of the flow rates using the RNG k-ε turbulence model compared to the flow rate measurements for two merging plumes with buoyancy flux ratio ψ=0.45.

The graphs show that the RNG k- ε model predicts this relationship more accurately than the standard k-ε model. This is thought to be due to the standard k- ε model over-predicting entrainment into the plumes and thus over-predicting the plume volume flux. An indication of the magnitude of this discrepancy is given in Table 2.

Table 2: *Percentage discrepancies between CFD predictions and experimental data*

RANS-based Turbulence Model	% discrepancy in slopes of the experimental and CFD results
k-ε	53.13
RNG k-ε	9.10

CONCLUSIONS

This paper demonstrates how important it is to select the appropriate turbulence model when simulating natural ventilation flows driven by buoyancy forces even in a very simple geometry. The results have been compared both qualitatively and quantitatively with experimental data. The general flow patterns and direction of the flow agree well with the experimental work for both turbulence models. In terms of the volume flow rate prediction in the plume, it is observed that the use of the RNG k-ε turbulence model shows better agreement with the experimental data compared with the standard k-ε turbulence model which showed discrepancies of up to 53%.

The results further confirm the generally widely felt view that turbulence is difficult to model, especially buoyancy produced turbulence. This investigation will be used as the basis for further study of the turbulence modelling of natural ventilation using large eddy simulation.

REFERENCES

Anderson, K. T. (1995), "Theoretical consideration on natural ventilation by thermal buoyancy", *ASHRAE Technical Data Bulletin,* vol. 11, No. 3, 48-62

Awbi, H. B. & Gan, G. (1992), "Simulation of solar induced ventilation, in: Proceedings of the Second World Renewable Energy Congress on Solar and Low Energy Architecture, *Pergamon Press, Oxford,* vol. 4.

Baines, W. D. (1983), "A technique for the measurement of volume flux in a plume", *Journal of Fluid Mechanics,* 132, 247-256.

Bansal, N. K., Rajesh M. & Bhandari M. S. (1993), "Solar chimney for enhanced stack ventilation, *Building and Environment*, 28 (3), 373-377.

Barozzi, G. S., Imbabi, M. S. E., Nobile E. & Sousa A. C. M. (1992), "Physical and numerical modelling for a solar chimney based ventilation system for buildings, *Building and Environment,* 27 (4), 433-445.

Bouchair, A. (1993) "Solar chimney for promoting cooling ventilation in southern Algeria, *Building Services Engineering Research Technology*¸15 (20), 81-93.

CHAM, PHOENICS VR. http://www.cham.co.uk. (2009)

Chen, Q. (1995), "Comparison of Different k-ε Models for Indoor Airflow Computations. *Numerical Heat Transfer*, 28(B): 353-369.

Cook, M. J. (1998), "An Evaluation of Computational Fluid Dynamics for Modelling Buoyancy-Driven Displacement Ventilation", PhD Thesis, De Montfort University.

Cook, M.J. & Lomas, K.J. (1997), "Guidance on the use of computational fluid dynamics for modelling buoyancy-driven flows", *Proc Building Simulation '97, Prague, Czech Republic*, 140-147.

Hunt, G. R. & Linden, P. F., (2001), "Steady-state flows in an enclosure ventilated by buoyancy forces assisted by wind", *J. Fluid. Mech.,* 426, 355-386.

Kaye, N. B. & Linden, P. F. (2004), "Coalescing axisymmetric turbulent plumes", *Journal of Fluid Mechanics*, vol. 502, 41-63.

Launder, B. E. & Spalding, D. B. (1974), "The numerical computation of turbulent flows", *Computer Methods in Applied Mechanics and Engineering*, vol. 3, 269-289.

Linden, P. F. (1999), "The fluid mechanics of natural ventilation", *Annual Review Fluid Mechanics,* 31, 201-238.

Linden, P.F., Lane-Serff, G.F. & Smeed, D.A. (1990), "Emptying filling boxes: the fluid mechanics of natural ventilation", *Journal of Fluid Mechanics*, 212, 309-335.

Murakami, S., Mochida, A., Ooka, R., Kato, S. & Iizuka, S. (1996), "Numerical Prediction of Flow around a Building with Various Turbulence Models: Comparison of k-ε EVM, ASM, DSM, and LES with Wind Tunnel Tests, *ASHRAE Transactions*, 102 (1), 741-753.

Murakami, S. (1998), "Overview of Turbulence Models Applied in CWE, 1997. *Journal of Wind Engineering and Industrial Aerodynamics,* 74-76: 1-24.

Pera, L. & Gebhart, B. (1975), "Laminar plume interaction". *Journal of Fluid Mechanics,* 65, 250-271.

Tan, C. C. (2000), "Solar induced ventilation", *PhD Thesis, School of Design and Environment,* National University of Singapore.

Van der Mass, J., Roulet, C. A., (1991), "Night time ventilation by stack effect", *ASHRAE Technical Data Bulletin,* 7 (1), 23-38.

Yakhot, V., Orszag, S. A., Thangam, S., Gatski, T. B. & Speziale, C. G. (1992), "Development of turbulence models for shear flows by a double expansion technique", *Physics of Fluids A*, Vol. 4, No. 7, 1510-1520.

NOMENCLATURE

A^*	effective opening area (m^2)
a_b	area of the lower opening (m^2)
a_t	area of the top opening (m^2)
b_G	Gaussian plume width (m)
b_T	top-hat plume width (m)
C_D	coefficient of discharge (-)
C_e	coefficient of expansion (-)
C_p	specific heat capacity (J/kg K)
$\hat{F}_1$	buoyancy flux in plume 1 (m^4/s^3)
$\hat{F}_2$	buoyancy flux in plume 2 (m^4/s^3)
g	acceleration due to gravity (m/s^2)
H	total height of computational domain (m)
h	mean interface height (m)
K_L	loss coefficient (-)
Q	volume flux (m^3/s)
q	heat source strenght (W)
v_G	Gaussian velocity (m/s)
v_T	top-hat value for velocity (m/s)
vel	velocity (m/s)
W	total heat source (W)
X_0	source separation (m)
z_m	plume merge height (m)
α	plume entrainment coefficient (-)
β	coefficient of thermal expansion (-)
ΔP_{loss}	pressure loss across the opening (Pa)
ρ	density (kg/m^3)
ψ	buoyancy flux ratio (-)
ξ	normalised interface height (h/H) (-)